RSC Advances

ROYAL SOCIETY OF CHEMISTRY

www.rsc.org/advances

High transparent and flexible silica/cellulose films with low coefficient of thermal expansion

Yuehan Wu, Xingzhong Zhang, Bin Li, Shilin Liu*

College of Food Science & Technology, Huazhong Agricultural University, Wuhan, Hubei, 430070 (China)

*Corresponding author: slliu2013@mail.hzau.edu.cn (S. Liu).

Abstract

High transparent and flexible silica/cellulose films with low thermal expansion coefficient have been prepared through in situ synthesis of silica in cellulose scaffolds by using Na_2SiO_3 as precursor. It indicated low content of silica in the composite films had an influence on the tensile strength of the composites. Furthermore, the composite films integrated the merits of cellulose and silica, the transmittance of the composite films in visible light region could be comparable with that of glass, but it was foldable. Moreover, the composite films had CTEs lower than 15 $ppm \cdot K^{-1}$. The composite films would be the perfect substrates for the future production of electronic devices, such as flexible displays, e-papers and could replace the costly conventional batch processes based on glass substrates currently used, and eventually to rollable and even foldable devices.

Keywords: cellulose, silica particle, scaffold, film, transparent

Introduction

There has been significant interest in flexible polymer materials with high thermal resistance, transparency, and low thermal expansion properties. This kind of material can be used in the emerging field of flexible electronics [1-5]. However, most of materials currently used have large coefficients of thermal expansion (CTEs, approx. 50 ppm·K^{-1}), and particular foldable plastics exhibit extremely large CTEs, in excess of 200 ppm·k^{-1}. Moreover, polymers usually have low glass transition temperatures (T_gs) where abrupt CTE changes are accompanied, which greatly limit their practical application in terms of the process temperature. In order to overcome these limitations, nanocomposites from hybrids of organic polymers and inorganic materials have attracted considerable interest. There also have been many studies on exploring the effect of nanoparticles incorporation with different chemical nature, size, and shape on the thermal and optical properties of polymers [6-11].

Biodegradable composites as a new kind of materials from renewable resources have attracted the attentions of researchers in diverse areas. These biohybrids not only display improved structural and functional properties, but also show remarkable advantages of biocompatibility, biodegradability and some other novel properties supported by either the biological or inorganic moieties [12-17]. Cellulose as the most abundant resource on earth has good mechanical and thermal stability properties at temperature ranging from room temperature to about 200 ^{o}C, furthermore, it has no T_gs because of the strong inter- and intra-molecular hydrogen bonds. It has been reported that scaffolds from cellulose nanofibers was a good matrix for the fabrication of composites with promising thermal stability [18-19], cellulose nanofiber or nanowhiskers were also good fillers for the preparation of composites with improved thermal properties [20-22]. However, there are considerable challenges in the

separating the native cellulose nanofibers from the macroscopic cellulose fibers or developing expensive large-scale fermentation technology for bacterial cellulose. Therefore, dissolution and regeneration of native cellulose has become an alternative pathway for the preparation of cellulose based functional materials.

We have put an intensive research on cellulose dissolving and construction of functional cellulose materials from the developed solvents. In our previous work, aqueous solvents containing alkaline and urea have been developed for cellulose dissolving [23-24]. The regenerated cellulose films prepared from LiOH/urea or NaOH/urea aqueous solution had porous structure, which could be used as scaffolds for the synthesis of inorganic nanoparticles [25-26] or curable organic prepolymers [27-28] in situ for the construction of functional cellulose materials, and the composites integrated the merits of the cellulose and the incorporated components. Inspired by the interesting characteristic, we attempted to develop a material with some properties like glass (e.g. high transmittance and low thermal expansion) by incorporation silica in the cellulose matrix. It indicated that the transmittance of the composites could be compared with that of the glass, but they were foldable and had good mechanical properties as well as low CTEs (CTE < 20 $ppm \cdot k^{-1}$). The straightforwardness of the fabrication of the cellulose based composite films represented not only a scientific term about the identifying compounds of natural origin and establishing economically efficient routes for the production of biodegradable and/or biocompatible composite materials, but also an emerging area of research aimed at the future design of green bioelectronics.

Experimental section

Chemicals. Native cellulose (Cotton linter, α-cellulose ≥ 95%) was supplied by Hubei Chemical Fiber Co. Ltd. (Xiangfan, China), and its viscosity-average molecular

weight (M_η) was about 1.07×10^5, which was determined in cadoxen at 25 ^oC. Other chemicals with analytical grade were supplied by the Sinopharm Chemical Reagent Co. Ltd (Shanghai, China). Deionized water was used for the experiments.

Preparation of regenerated cellulose (RC) films and composite films. The freezing-thawing method was used for cellulose dissolving. Briefly, powder-like filter paper (Native cellulose) was dispersed into aqueous lithium hydroxide/urea solution (4.6 wt %/15.0 wt %), and then put it in a refrigerator, after it had been frozen, took it out and thawed at room temperature to obtain a transparent cellulose solution (5wt%). The resultant cellulose solution was subjected to centrifugation at 7,500 rpm and 15^oC for 10 min to eliminate some bubbles in the viscous solution. The viscous bubble-free solution was cast on a glass plate and the thickness of the solution was controlled to be about 0.9 mm, and then immersed it into coagulation bath containing 80 v% ethanol to regenerate for 10 min. The regenerated cellulose films (RC) were washed with deionized water and then immersed into Na_2SiO_3 solution for 24h, and subsequently, treated with mixed ethanol and H_2SO_4 (2M) solution for 20 min. The composite films were washed with deionized water and dried at ambient conditions. The composite films prepared from Na_2SiO_3 solution with concentration of 2 wt%, 5 wt%, 10 wt%, and 15 wt% was coded as CMS-2, CMS-5, CMS-10, and CMS-15, respectively. The regenerated cellulose film that was not treated with Na_2SiO_3 solution was coded as RC.

Characterization

X-ray diffractometry of the regenerated cellulose film and composite films were carried out on reflection mode (Rigaku RINT 2000, Japan) with Ni-filtered CuKa radiation. Fourier-transform infrared spectra (FT-IR) of the samples were recorded with an FT-IR spectroscopy (FT-IR 615, Japan). The samples were ground into

powders, mixed with KBr, and pressed to form a sample disk for FT-IR measurements. For transmission electron microscopy (TEM) test, the specimens were embedded in a poly (methylmethacrylate–butylmethacrylate) (PMMABMA) resin and then cut with a Leica Ultracut-E by using a glass knife. The sections of approximately 100 nm thickness were mounted on a grid with carbon support, and then disembodied by removing the resin with acetone. The section was then examined with a JEOL-1010 apparatus. Scanning electron microscopy (SEM) observation of the surfaces of the RC and composites was carried out by using a Hitachi S-4800 microscope. Prior to analysis, samples were cut into small pieces from the prepared samples and coated with a thin layer of evaporated gold. Thermal gravimetric analysis (TGA) was carried out by using a thermogravimetric analysis (Ulvac TGD 9600). The samples were cut into powders and about 30 mg of the powder was placed in a platinum pan and heated from 20 to 700 ^{o}C at a rate of 10 K•min^{-1} in nitrogen atmosphere. Optical transmittance (*T*r) of the cellulose film and composite films were measured with a Shimadzu UVmini-1240 apparatus at wavelengths ranging from 200 to 1000 nm. The mechanical properties of the films were characterized with a tensile tester (CMT 6503, Shenzhen SANS Test machine Co. Ltd, China) according to ASTM/D638-91 at a speed of 5 mm·min^{-1}, and five samples were tests for each set of samples. The coefficients of thermal expansion (CTEs) were carried out on a thermomechanical analyzer (TMA/SS6000, SII Nanotechnology Inc.). Specimens were 20 mm long and 5mm wide with a 15mm span. The measurements were carried out from 30 to 120°C by elevating the temperature at a rate of 10°C·min^{-1} in air in tensile mode under a load of 2g. The linear coefficient of thermal expansion (CTEs) could be expressed by:

$$CTE_s = \frac{1}{L_0}\frac{\Delta L}{\Delta T}$$

where ΔL was the change in length of the test specimen due to heating, L_0 was the initial length of the test specimen at room temperature, and ΔT was the temperature difference over which the change in the length of the specimen was measured. CTEs could be obtained from the slope of the curve obtained when the change in the films length, ΔL, was represented as a function of the temperature, T. The CTE values were determined in the fourth run.

Results and discussion

The composite films containing silica were prepared by in situ synthesis according to the scheme in Fig. 1. The RC films displayed homogeneous macroporous structure, as it was shown in Fig. 1. This unique structure was due to the phase separation of the cellulose solution during the regenerating process, where solvent-rich regions contributed to the pore formation. The N_2 adsorption-desorption isotherm of the cellulose hydrogel after being freeze-dried indicated the formation of a continuity of the pore size distribution of macropores, and S_{BET} inferred from the N_2 adsorption isotherm by using a Brunauer-Emmett-Teller analysis of the amount of gas adsorbed at P/P_0 between 0.05 and 0.3 was about 270 m^2/g. When the cellulose hydrogel films were immersed into Na_2SiO_3 solution, the solution could be readily impregnated into the cellulose scaffolds through the pores. When the films were treated with the mixed H_2SO_4 and ethanol aqueous solution, Na_2SiO_3 transformed into silica gels immediately, and the transparency of the composite films was improved after the reaction process when compared with that of the pristine cellulose films. It must be noted that the composite films would be opaque when the cellulose hydrogel films containing Na_2SiO_3 were treated with ethanol first and then followed with H_2SO_4.

In order to clarify this interesting phenomenon, the microstructure of the composite films after being freeze-dried were characterized with SEM. Fig. 2 shows the

morphologies of the composites after being freeze-dried. It was clear that silica components conferred an obvious change in the microstructure of the composites compared with that of pristine cellulose film. In all of the samples, obvious macropores had a diameter mainly in the 100 nm range, which was smaller than that of the cellulose film. It indicated that silica components had an obvious influence on the microstructure of the composites. There was also evidence that all the samples contained an additional mesoporous sub-structure, consisting of fibrils with diameter about 30 nm, which was more uniform than that of cellulose films. This interesting phenomenon could be ascribed to the contribution of silica components in the cellulose matrix. However, the silica particles could be hardly detected. It would be resulted from the fact that the silica sheath was synthesized on the surface of the cellulose nanofibrils. While for the cellulose hydrogel film containing Na_2SiO_3 was treated with ethanol first and then followed with H_2SO_4, silica particles were formed in the cellulose matrix, see supporting information (FS1). In order to further clarify the structure of the composite films, TEM test was carried out by ultrathin sectioning of resin-embedded composite films, and then followed by removal of the resin on the TEM grid. Fig. 3 shows the micrographs of the composite films. Silica nanoparticles with a mean particle size about 20 nm were dispersed uniformly in the cellulose matrix. With the increase of the concentration of Na_2SiO_3 solution, the particle size changed slightly, suggesting that the network of cellulose matrix could act as reacting sites not only for the synthesis of the silica nanoparticles, but also could keep the nanoparticles from growing into large size. For the cellulose hydrogel film containing Na_2SiO_3 was treated with ethanol first and then followed with H_2SO_4, silica particles with larger particle size were formed in the cellulose matrix, see supporting information (FS1).

Fig. 4 shows the XRD of the RC and the composite films. The peaks at 2θ = 12.1, 20.3, and 21.8° were corresponding to the (1$\bar{1}$0), (110), and (200) crystalline planes of cellulose II crystalline, respectively [29]. It was worthwhile to be noted that in addition to the diffraction peaks of cellulose II, there was no diffraction peak of silica observed in the composite films. It is suggested that the silica in the composite films existed as amorphous. The results were consistent with the reported conclusions about preparation of SiO_2 from liquid-phase silica source, such as water glass [30]. FT-IR spectroscopy was used to characterize the cellulose and silica/cellulose composite films at the molecular structure level. The spectra of some selected samples were shown in Fig. 5. The strong and broad band centered at ~3400 cm^{-1} was assigned to the stretching mode of -OH groups involved in different hydrogen-bonding interactions. They were correlated with -OH of cellulose and molecular water (in the H-O-H deformation region, at ~1648cm^{-1}) [31]. The strongest band with the maximum absorption at ~1070 cm^{-1} was assigned to the antisymmetric Si-O-Si stretching mode. The corresponding symmetric mode appeared at ~800cm^{-1}. The ν_{as} Si-O-Si band was the most informative on the structure of the silica [32].

The thermal stability and degradation profile of the RC and composite films was assessed by thermogravimetry and was shown in Fig. 6. A small weight loss of ~5% around 80°C was assigned to the release of moisture from the samples. The pure RC film showed two obvious weight loss slopes with elevating temperature. The first weight loss was found in the temperature ranged from 300~350 °C, which was ascribed to the onset decomposition of cellulose. The second weight loss peak at 420~540 °C was attributed to the decomposition of cellulose. The thermal stability of the composites apparently decreased because of the destruction of the microstructure of cellulose. With an increase of the content of the silica, the initial decomposition

195 temperature of the composites shifted to lower temperatures. The first weight loss
196 stage for the pure RC film was around 326 ^{o}C, which decreased to about 250 ^{o}C when
197 the silica nanoparticles were loaded, and it shifted to lower temperature with the
198 increasing of the incorporated silica components, which indicated the formation of the
199 composites with partially disrupting the interaction in cellulose matrix. It was worth
200 noting that the thermal decomposition temperature of the composite films was higher
201 than those of the synthetic polymers that often used in photoelectric devices, such as
202 PMMA(~170^{o}C) or PVC(~200^{o}C).

203 An extremely important property of the composite films was their improved
204 optical transparency. Fig. 7 illustrated the optical transmittance spectra in the visible
205 region of the RC and composite films with different silica loadings. The transmittance
206 of the RC films at the 550 nm wavelength was 83%, and the transparency was
207 improved to 92 % with the loading of low content of silica nanoparticles. Surprisingly,
208 since the regular transmittance of glass with the thickness about 1.35 mm was 93%
209 including surface reflection. It indicated that the optical transmittance of the
210 composite films was comparable to that of glass. For a transparent polymer composite
211 with dispersed inorganic fillers, the optical property was described as:

212 $$\frac{I}{I_0} \equiv \exp\left[-\frac{V_p \chi r^3}{4\lambda^4}\left(\frac{n_p}{n_m}-1\right)\right]$$

213 Where χ was the optical path length, V_p was the particle volume fraction, r was the
214 particle radius, λ was the light wavelength, and n_p and n_m were the refractive indices
215 of the fillers and matrix, respectively. The difference of the refractive index of the
216 fillers and matrix played an important role in controlling the optical transmittance of
217 the composite films. It was known that the refractive index of cellulose and silica
218 were about 1.47 and 1.63, respectively. Therefore, when the silica nanoparticles were

impregnated into the cellulose matrix, the composite films displayed improved transmittance due to the smaller difference in n_p and n_m. Nogi et al. reported that acetylation of cellulose nanofibers could decrease the refractive index and made it close to the refractive index of resin, and high transparency composite could be obtained from these two materials. The unique network structure of the RC matrix also contributed to the improvement of the transmittance of the composite films. The porous structure of the cellulose matrix could control the particle size of silica particles and made their distribution in cellulose matrix homogeneously, resulting in the increment of the affinity between silica particles and cellulose matrix, which should also relate to the high transparency. Since silica particles and cellulose were hydrophilic, the affinity of the silica particles surface and cellulose matrix was increased, allowing the silica particles formed into the cavities of the cellulose matrix tightly. As a result, scattering of the visible light at the interface of the silica particles decreased. The introduction of excess of silica particles in the cellulose matrix did not result in high transparency of the composite films, but the composite films became brittle.

The typical stress-strain curves of the RC and composite films were shown in Fig. 8a. Pure RC film had a tensile strength about 81 MPa with the elongation at break about 10.7%, while for the composite films containing lower content of silica about 4.5 wt%, the tensile strength of the composite film increased from 81 to 95 MPa, with the decreasing of the elongation at break to about 6%, while for the composite films with higher content of silica, the tensile strength decreased from 95 MPa to 86 MPa, but the tensile strength could be compared to that of pure RC. The decrease in the tensile strength of the composite films prepared from different concentration of the silica precursor would be resulted in two factors. The first one was that the content of

244 silica in the composite films increased with the increasing the concentration of the
245 precursor, higher content silica would destroy the network structure of the composite
246 films, the second factor could be ascribed the increased particle size of the silica
247 particles, in the TEM results, it could be detected that the particles size of silica
248 increased with the increasing the precursor concentration, the larger sized silica
249 particles with higher content could form stress concentration in the composite.
250 Therefore, the tensile strength decreased with the increasing the silica fillers. The
251 Young's modulus of the composite films increased slightly and then decreased, and
252 there was no obvious difference in the Young's modulus of the composites, as it was
253 shown in Figure 8b. Furthermore, the result for composite films demonstrated clearly
254 that unbendable silica materials became ductile by reinforcement with cellulose
255 nanofibrils networks, suggesting the network structures of cellulose scaffolds
256 suppressing the crack propagation in the composite films, indicating that the
257 composite films integrated the virtues of silica and cellulose, suppressing break and
258 generating attractive tensile strength and reliably foldability. The flexibility is an
259 essential characteristic not only for future electronic devices such as displays and
260 solar cells, but also as materials suitable for roll-to-roll production processes.

261 The thermal expansion properties of the RC and composite films were investigated
262 with a thermal mechanical analysis chart, the slope of which reflected the coefficient
263 of linear thermal expansion. The obtained length-normalized charts were shown in Fig.
264 9, and the corresponding CTEs of the samples from the fourth run were shown in Fig.
265 10. The CTE of the RC films was about 16 ppm•K^{-1} over a temperature ranged from
266 30 to 100^{o}C. The CTEs of the composite films was lower than that of the RC film, and
267 it decreased with the increasing the content of silica in the composites. It was worth
268 noting that for the CMS-15 composite film with silica content about 11.2%, the CTEs

was as low as 12 ppm•K^{-1}, which was lower than many transparent polymer films current used. Furthermore, the composite film was foldable in this state. It was well known that the interaction between a polymer matrix and a filler surface caused lower CTEs. In our work, the silica nanoparticles were synthesized around the cellulose nanofibriles. When the composites were heated, the silica and cellulose matrix would be expanded. However, the silica has lower coefficient of thermal expansion than that of cellulose, therefore the thermal expansion behavior of the cellulose matrix was limited by the silica components. Consequently, the composite films would be deformed difficultly by the thermal expansion of the composites. It had been also pointed out that it was of great importance to making the nanofiber network interaction strong to restrict the thermal expansion of the matrix so as to the improvement of the CTE in acetyl composite. In the currently practical application, transparent film with a low CTE, typically less than 20 ppm•K^{-1}, was desirable to match the thermal expansion of the substrates to the deposited OLED layers. This novel property could be explained by the unique network structure of the cellulose film, and the induced thermal stresses were small enough to be almost completely constrained by the rigid networks of cellulose matrix. It would be a promising technology for the preparation of advanced cellulose composite films for functional applications.

Conclusions

In summary, flexible, transparent composite films with the structural robustness were prepared successfully by using a facile process. The composite films integrated the merits of the cellulose and silica, and they were mechanically strong, flexible, and with obvious low CTEs. The incorporated silica had little influence on the thermal properties and obvious influence on the mechanical properties of the composite films,

and the composite films had high optical transmittance, the transmittance at 550 nm was higher than 80%. The achievements suggested that the prepared composite films were potentially feasible to be implemented in a wide range of the practical applications owing to its desirable properties including mechanical flexibility, optical transparency, and mechanical robustness as well as low CTEs properties.

Acknowledgements

This work was supported by the National Natural Science Foundation of China (No. 51273085 and 51003043), and the project by the Fundamental Research Funds for the Central Universities (2014PY024).

References

1. M. C. Choi, Y. Kim and C.S. Ha, *Prog. Polym. Sci.*, 2008, **33**, 581-630.
2. D. Ghosh, P. GhoshP, M. Tanemura, A. Haysahi, Y. Hayashi, K. Shinji, N. Miura, M. Z. Yusop and T. Asaka, *Chem. Commun.*, 2011, **47**, 4980-4982.
3. B. H. Lee, S. H. Park, H. Back and K. Lee, Adv. Func. Mater., 2011, **21**, 487-493.
4. W. A. MacDonald, *J. Mater. Chem.*, 2004, **14**, 4-10.
5. L. C. Tomé, R. J. Pinto, E. Trovatti, C. S. Freire, A. J. Silvestre, C. P. Neto and A. Gandini, *Green. Chem.*, 2011 **13**, 419-427.
6. H. Althues, J. Henle and S. Kaskel, *Chem. Soc. Rev.*, 2007, **36,** 1454-1465.
7. J. Opatkiewicz, M. C. LeMieux and Z. Bao, *ACS Nano.*, 2010, **4**, 2975-2978.
8. I. Perez-Baena, I. Loinaz, D. Padro, I. García, H. J. Grande and I. Odriozola, *J. Mater. Chem.*, 2010, **20**, 6916-6922.
9. Y. Rao and T. N. Blanton, *Macromolecules*, 2008, **41**, 935-941.
10. G. Wu, H. Xu and T. Zhou, *Polymer*, 2010, **51**, 3560-3567.
11. Y. Yin and C. Wang, *J. Sol-Gel Sci. Technol.*, 2011, **59**, 36-42.
12. H. Fukuzumi, T. Saito, T. Iwata, Y. Kumamoto and A. Isogai, *Biomacromolecules*, 2008, **10**,162-165.
13. S. Ifuku, S. Morooka, A. N. Nakagaito, M. Morimoto and H. Saimoto, *Green Chem.*, 2011,**13**, 1708-1711.
14. M. Nogi and H. Yano, *Adv. Mater.*, 2008, **20**, 1849-1852.
15. M. Nogi and H. Yano, *Appl. Phys. Lett.*, 2009, **94**, 233-117.
16. M. Nogi, S. Iwamoto, A. N. Nakagaito and H. Yano, *Adv. Mater.*, 2009, **21**, 1595-1598.
17. L. Carro, E. Hablot and T. Coradin, *J. Sol-Gel Sci. Technol.*, 2014, **70**, 263-271.
18. C. Y. Yan, J. Wang, W. Kang, M. Cui, X. Wang, C. Y. Foo, K. J. Chee and P. S.

Lee, *Adv. Mater.*, 2014, **26**, 2022–2027.

19. Z. Fang, H. Zhu, Y. Yuan, D. Ha, S. Zhu, C. Preston, Q. Chen, Y. Li, X. Han, S. Lee, G. Chen, T. Li, J. Munday, J. Huang and L. Hu, *Nano Lett.*, 2014, **14**, 765−773.
20. N. Ucar, O. Ayaz, E. Bahar, Y. Wang, M. Oksuz, A. Onen, M. Ucar and A. Demir, *Text. Res. J.*, 2013, **83**, 1335-1344.
21. M. F. Rosa, E. S. Medeiros, J. A. Malmonge, K. S. Gregorski, D. F. Wood, L. H. C. Mattoso, G. Glenn, W. J. Orts and S. H. Imam, *Carbohydr. Polym.*, 2010, **81**, 83–92.
22. A. J. Svagan, M. A. S. Azizi Samir and L. A. Berglund, *Biomacromolecules*, 2007, **8**, 2556–2563.
23. S. Liu and L. Zhang, *Cellulose*, 2009, **16**, 189-198.
24. J. Zhou, S. Liu, J. Qi and L. Zhang, *J. Appl. Polym. Sci.*, 2006, **101**, 3600-3608.
25. S. Liu, J. Zhou and L. Zhang, *J. Phys. Chem. C.,* 2011, **115**, 3602-3611.
26. S. Liu, Q. Yan, D. Tao, T. Yu and X. Liu, *Carbohydr. Polym.*, 2012, **89**, 551-557.
27. S. Liu, D. Tao, T. Yu, H. Shu, R. Liu and X. Liu, *Cellulose*, 2013, **20**, 907-918.
28. W. Li, Y. Wu, W. Liang, B. Li and S. Liu, *ACS Appl. Mater. Interfaces.*, 2014, **6**, 5726-5734.
29. L. Zhang, D. Ruan and J. Zhou, *Ind. Eng. Chem. Res.*, 2001, **40**, 5923-5928.
30. S. L. Pan, J. J. Zhang and G. Z. Song, *Mater. Sci. Technol.,* 2009, **25**, 1437-1441.
31. C. J. Lee, G. S. Kim and S. H. J. Hyun, *Mater. Sci.*, 2002, **37**, 2237-2241.
32. A. Fidalgo and L M. J. Ilharco, *Non-Cryst. Solids.*, 2011, **283**, 144-154.

351 **Table 1.** Properties of the cellulose and silica/cellulose composite films prepared from Na_2SiO_3 solution with different concentrations.
352

Sample	Silica content (wt%)	Transmittance at 550 nm (%)	Strain (%)	Stress (MPa)	Young's modulous (Gpa)	CTE ($ppm \cdot K^{-1}$)
RC	0	86	10.84±0.47	82 ± 3.89	3.96±0.75	15.92±0.41
CMS-2	4.53	90	6.72 ± 0.79	96 ± 2.95	4.33 ± 0.82	14.90±0.57
CMS-5	5.83	89	8.54 ± 0.15	95 ± 2.16	4.39 ± 0.36	13.41±0.64
CMS-10	9.44	89	4.67 ± 0.96	69 ± 2.20	3.84 ± 0.71	12.66±0.36
CMS-15	11.27	91	2.76 ± 0.39	86± 3.74	4.17 ± 0.56	12.14±0.41

353

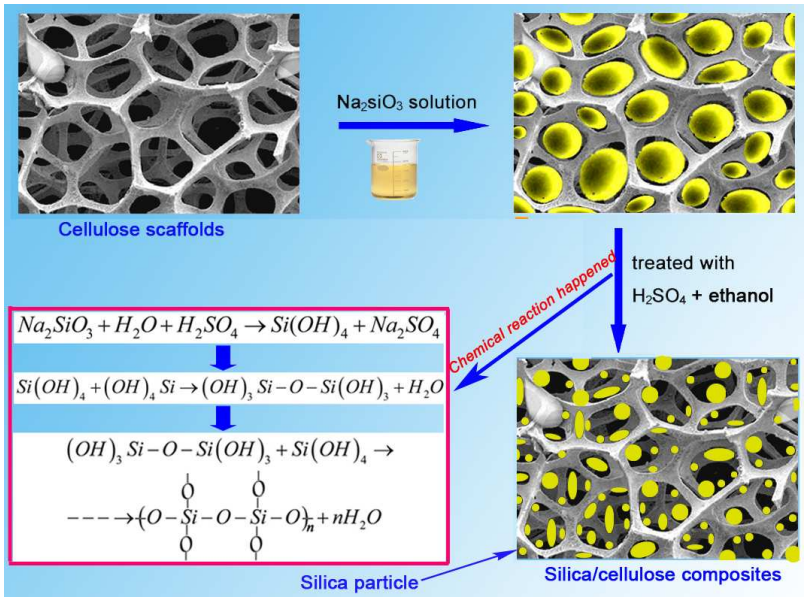

354

355 **Schedule 1.** The process for the preparation of silica/cellulose composite films.

356

357

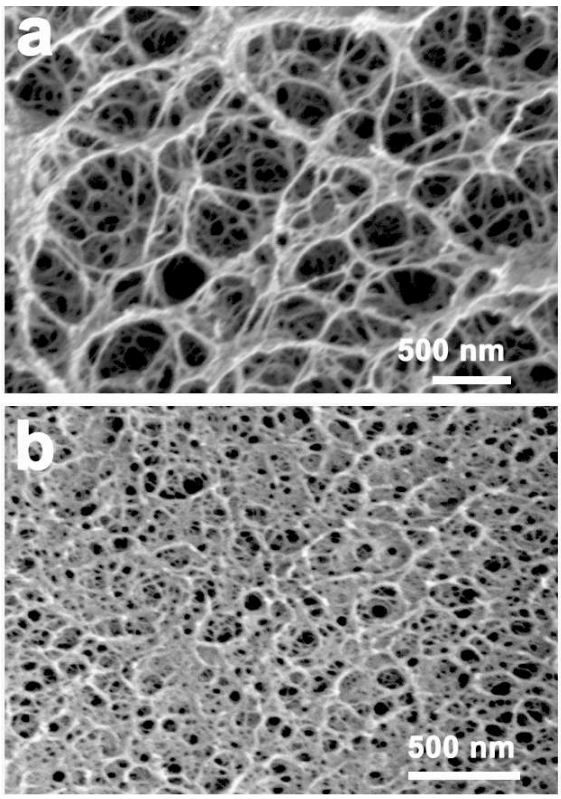

358

359

360 **Fig.1** SEM images of the RC film after being freeze-dried, a and b were for the

361 surface and cross-section of the film, respectively.

362

363

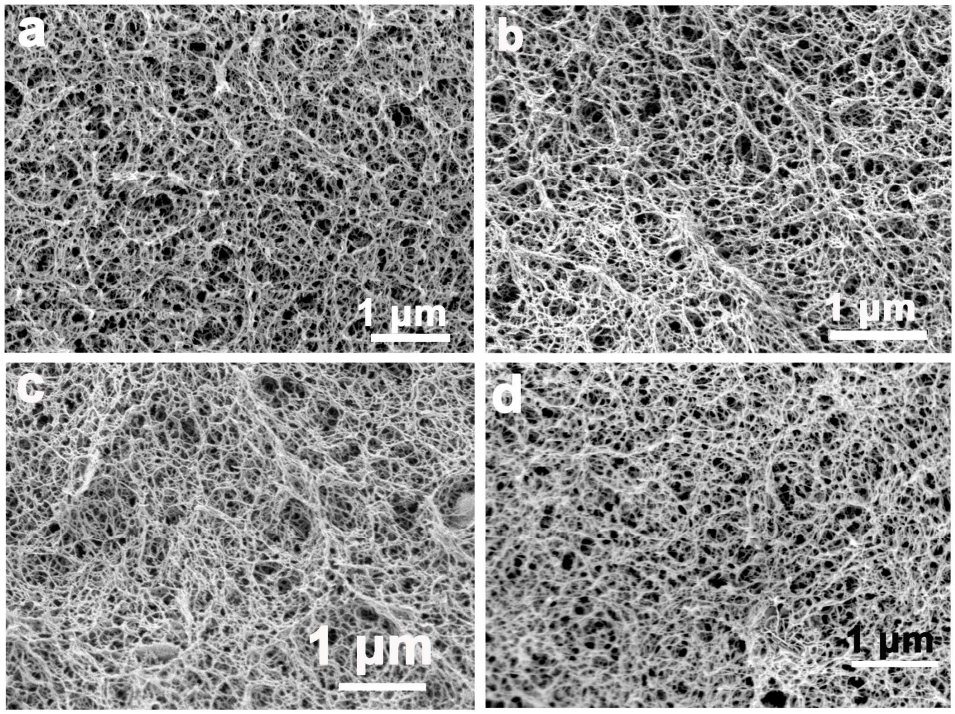

364

365 **Fig. 2** SEM images of the silica/cellulose composite films after being freeze-dried, a,

366 b, c, d were for CMS-2, CMS-5, CMS-10, and CMS-15, respectively.

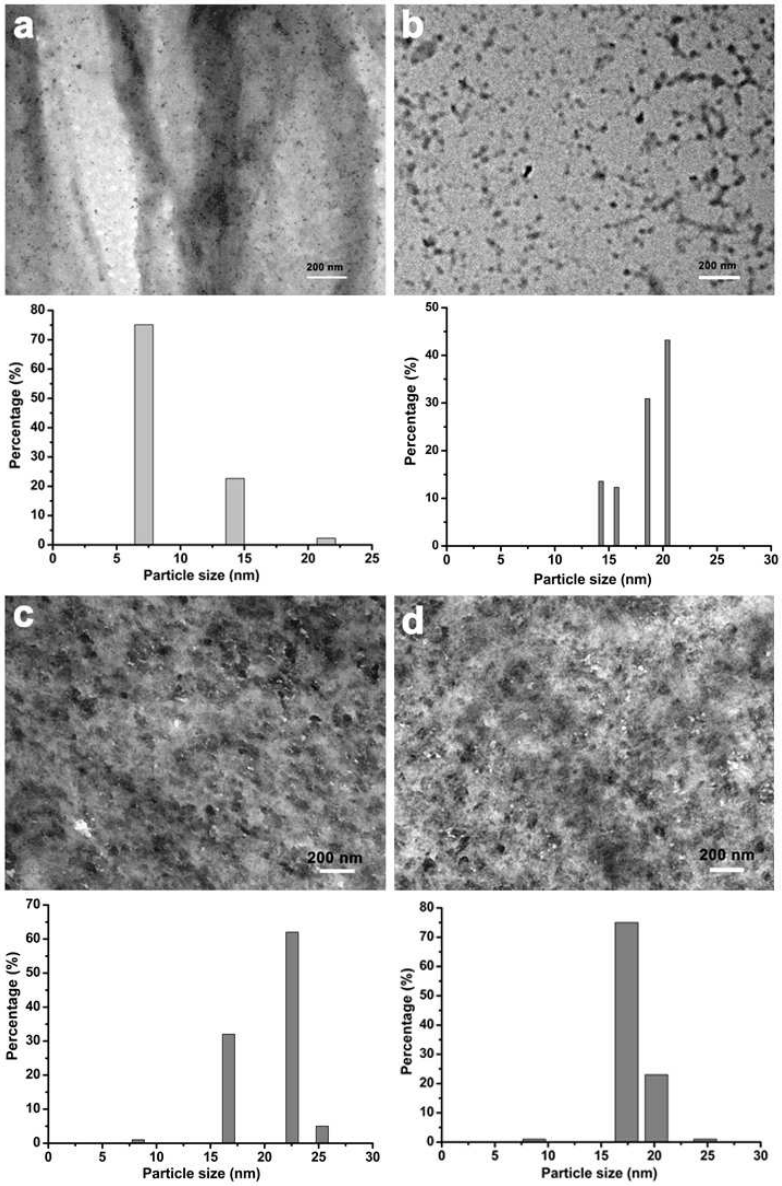

367

368 **Fig. 3** Ultrathin-section TEM images of the silica/cellulose composite films and the
369 particle size distribution, the particle size distribution was counted from at least 500
370 particles, a, b, c, d were for CMS-2, CMS-5, CMS-10, and CMS-15, respectively.

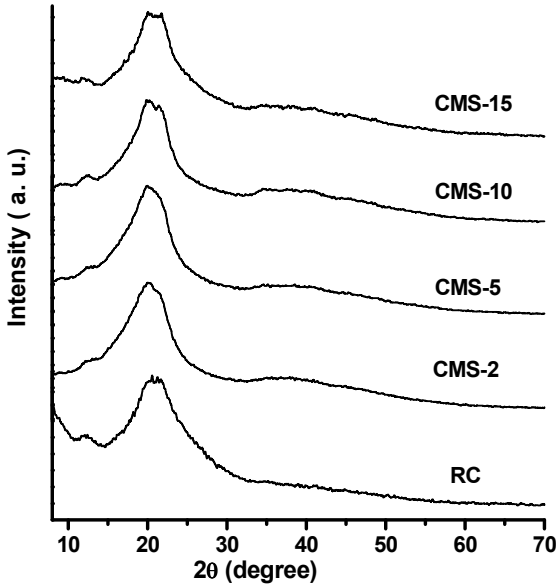

371

372 **Fig. 4** XRD patterns of regenerated cellulose film and composite films.

373

374

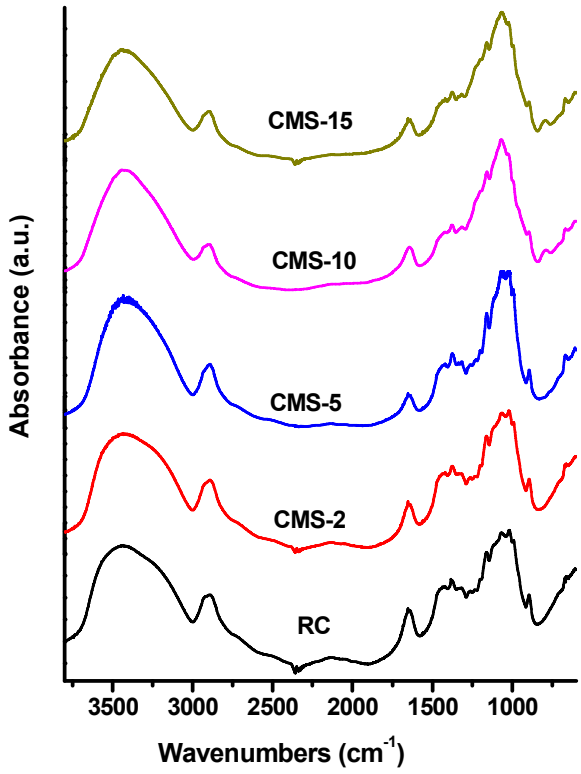

375

376 **Fig. 5** FT-IR spectra of the RC and silica/cellulose composite films.

377

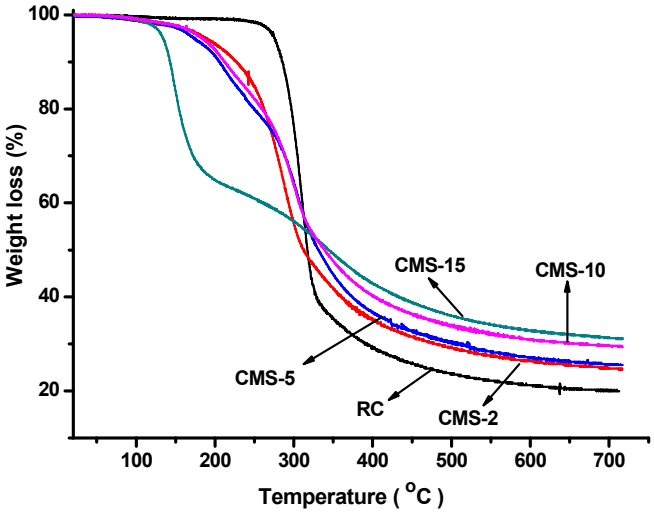

Fig. 6 Thermogravimetric curves for the RC and silica/cellulose composite films.

383

384

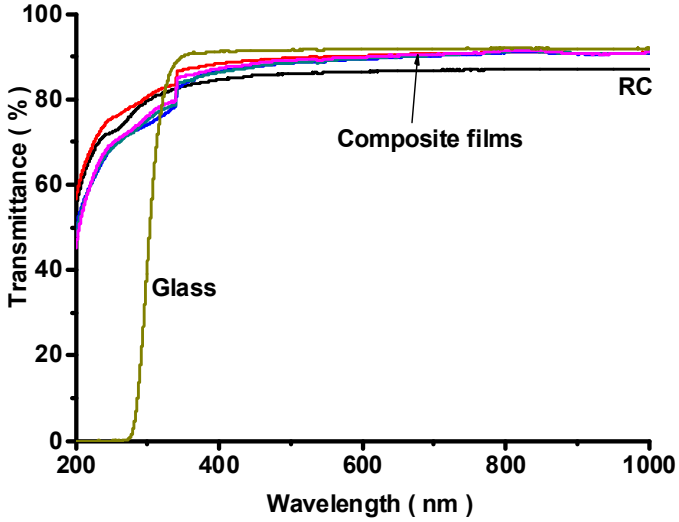

385 **Fig. 7** Transmittance of the RC and composite films in the wavelength from 200 to

386 1000 nm.

387

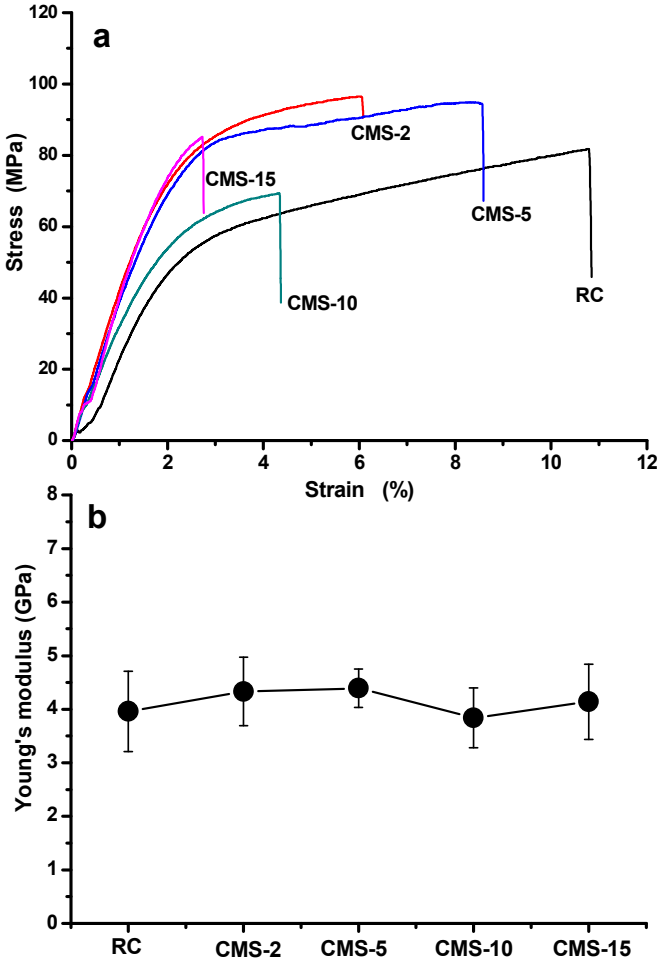

388

389 **Fig. 8** Stress-strain curves (a) and Young's modulus of the RC and silica/cellulose

390 composite films prepared fromNa_2SiO_3 solution with different concentration.

391

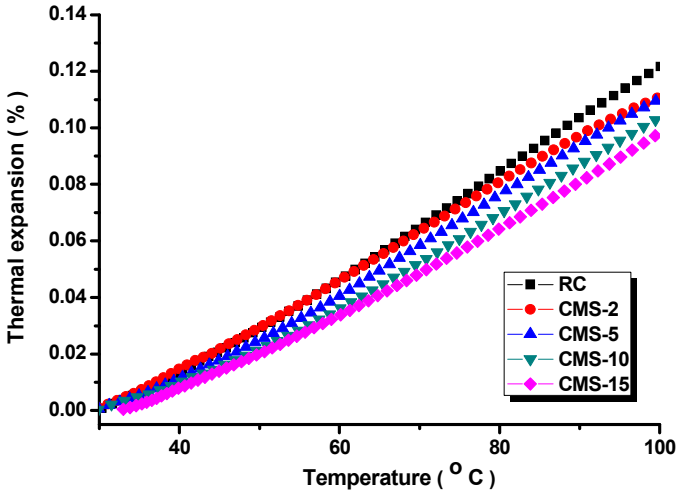

392

393 **Fig. 9** Thermal expansion curves of the RC and silica/cellulose composite films in the

394 temperature ranging from 30 to 100 °C, the data used for the figure was obtained from

395 the fourth run.

396

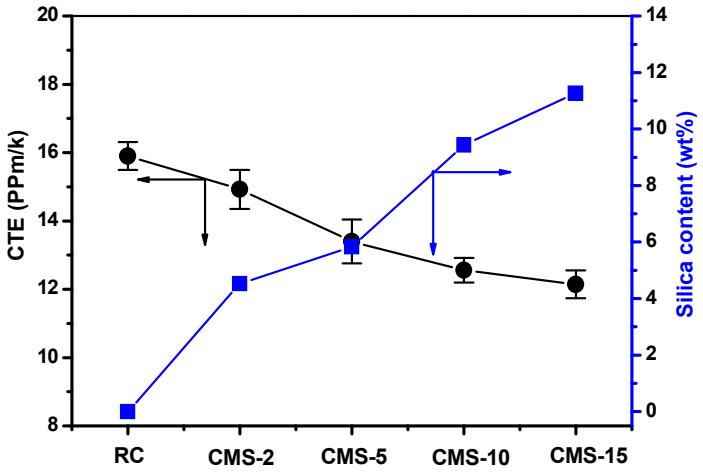

397

398 **Fig. 10** The relationship between the silica content and the coefficient of thermal

399 expansion of the RC and composite films. The CTE values were determined in the

400 fourth run.

401

402

403

404

405 **For table of content use only**

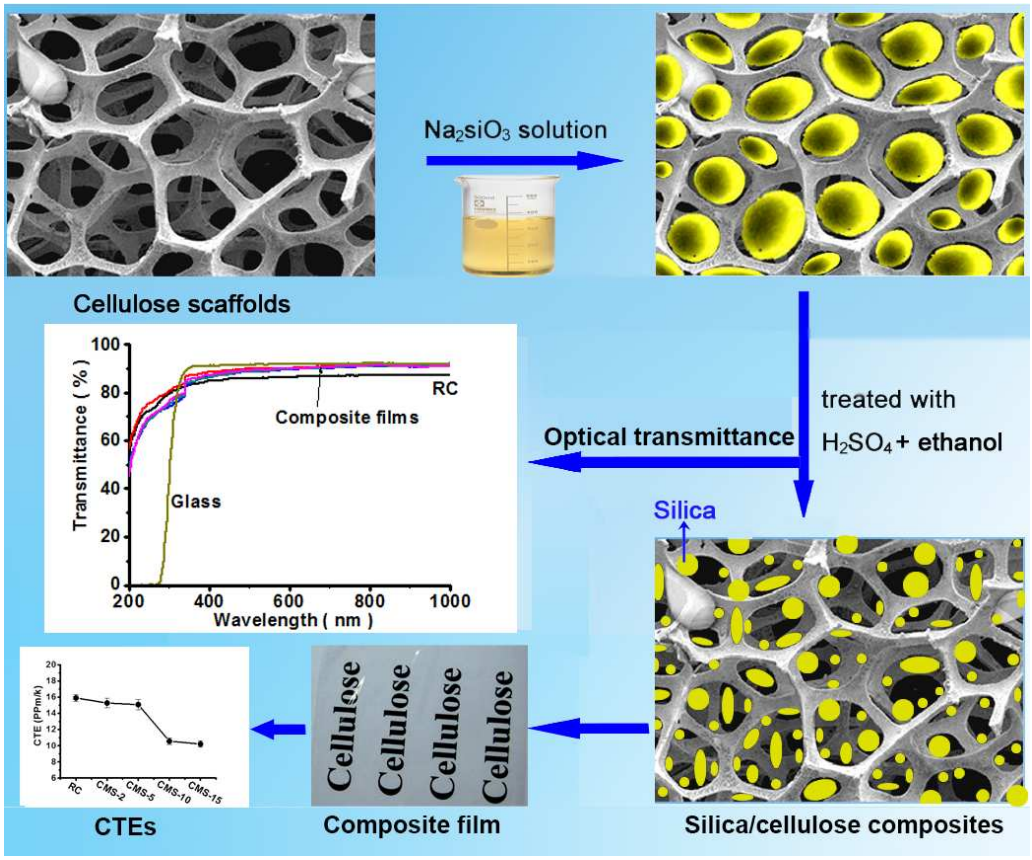

406